Ⓔ

Fluid Injection and Seismic Activity in the Northern Montney Play, British Columbia, Canada, with Special Reference to the 17 August 2015 M_w 4.6 Induced Earthquake

by Alireza Babaie Mahani, Ryan Schultz, Honn Kao, Dan Walker, Jeff Johnson, and Carlos Salas

Abstract In this article, we analyzed the recent seismic activity in the northern Montney Play of British Columbia in 2015 and its connection with fluid injection (hydraulic fracturing and long-term injection of gas and wastewater disposal) in the region. The earthquake sequence used in this study includes 676 events from 3 October 2014 to 31 December 2015 from the Progress Energy earthquake catalog with moment magnitude as small as 1. Spatial and temporal correlation of seismic activity with the fluid injection in the region revealed that these events are better correlated with hydraulic fracturing (correlation coefficient of ∼0.17 at confidence level close to 99.7%, with a lag time between 0 and 2 days) than other types of injection. Using the double-difference relocation technique, we obtained depth constraints for some of the events for which supplementary, industry-provided waveforms were available. The depths of these events range from 0.5 to 2.5 km and are mostly constrained above the target zone where hydraulic fracturing was taking place. The best-fit moment tensor solution for the event on 17 August 2015 gives a moment magnitude of 4.6 and a predominantly thrust mechanism in the northwest–southeast direction with a shallow focal depth of 4 km. This is consistent with that obtained through double-difference relocation for this event (1.3 km), given the depth uncertainty of the moment tensor inversion.

Electronic Supplement: Tables of injection volumes and seismicity parameters, and figure of monthly distribution of seismic events and location of fluid injection sites in the vicinity of the 17 August 2015 M_w 4.6 event.

Introduction

Earthquakes in the western Canadian sedimentary basin associated with various anthropogenic activities such as hydrocarbon production (Wetmiller, 1986; Baranova *et al.*, 1999), water flooding (Horner *et al.*, 1994), wastewater disposal (Schultz *et al.*, 2014), and hydraulic fracturing (Farahbod *et al.*, 2015; Schultz, Mei, *et al.*, 2015; Schultz, Stern, *et al.*, 2015) became a topic of focus in the provinces of Alberta and British Columbia. After both the number and size of induced earthquakes increased significantly in recent years, regulations have been put in place to monitor and control activities in certain areas where abnormal seismic patterns were observed (see Data and Resources). It is important to study induced seismicity because an increase in the number of events associated with oil and gas activity can have a significant impact on the regional seismic-hazard assessment, especially at sites close to the sources (Atkinson *et al.*, 2015). Moreover, larger induced events can have the

potential of generating ground motion that is above the damage threshold, although this has not been observed in Canada. The largest event to date that occurred in the vicinity of oil and gas operations was the 17 August 2015 earthquake with a moment magnitude (M_w) of 4.6 (see Data and Resources) in the northern Montney Play of British Columbia (NMP BC) where multistage hydraulic fracturing and long-term fluid injection have been taking place for decades (see Data and Resources).

Unfortunately, the station density of regional seismograph networks in the NMP BC is insufficient for near-field (<50 km) ground-motion measurements despite the significant improvement made through a joint effort by the Natural Resources Canada (NRCan), the BC Oil and Gas Commission, Geoscience BC, and the Canadian Association of Petroleum Producers since 2013 (Babaie Mahani *et al.*, 2016). Meanwhile, private companies established

their own seismograph networks for earthquake monitoring near injection sites. At this moment, these private datasets are not easily obtainable, and therefore their potential to improve our understanding of induced seismicity has been underdeveloped to date.

The goal of this article is to take advantage of two industry-provided datasets from broadband seismograph networks in the shale gas production areas, combined with the available public data from regional networks, to investigate the connection between seismic activity and fluid injection in the NMP BC in 2015. We start by compiling seismicity and injection catalogs for the area surrounding the M_w 4.6 event. We then analyze the spatial and temporal correlation of seismicity with fluid injection in the area, supplemented with statistical correlation between injection and seismicity. The hypocentral parameters of events with supplementary, industry-provided waveforms are determined through double-difference inversion to constrain the depth of the events, relative source locations, and their proximity to a nearby hydraulic fracturing completion pad. Finally, the focal mechanism of the 17 August 2015 M_w 4.6 earthquake is determined through moment tensor inversion.

Seismicity in Northeast British Columbia

Seismic activity in northeast British Columbia (NE BC) can be observed in clusters to the east of the Rocky Mountain fold-and-thrust belt (RMFTB; Fig. 1). These clusters occur in areas associated with fluid injection such as water flooding, hydraulic fracturing, and wastewater disposal (Horner *et al.*, 1994; Babaie Mahani *et al.*, 2016). Several events of magnitude 4 and higher (stars in Fig. 1) occurred in the past. The largest event to date occurred on 17 August 2015 in the NMP BC with an M_w of 4.6. For more information on seismic activity in NE BC, readers are referred to Babaie Mahani *et al.* (2016).

Figure 1 shows seismicity in NE BC (55°–58° N, 120°–125° W) from 1985 to 2016 as reported in the NRCan earthquake catalog. The black outline defines the Montney Play, which is the gas-bearing formation that extends from central Alberta to NE BC. The conventional sandstone and dolostone reservoirs of the Montney Formation have been the target of oil and gas explorations since 1950s (see Data and Resources). The unconventional siltstone resource of the Montney Formation, however, remained undeveloped until 2005 when advances in horizontal drilling and multistage hydraulic fracturing made its economic development possible (see Data and Resources). Thousands of wells have been drilled in the region since the initiation of unconventional development of oil and gas.

In addition to the regional seismograph network operated by NRCan and its partners, we used data from two private seismograph networks in the NMP BC (Fig. 1). The Progress Energy network has been in operation since October 2014 to monitor the relationship between local earthquakes and hydraulic fracturing, whereas the Canadian Natural Resources Limited (CNRL) seismograph network was put in place in March 2014 to monitor any events related to a nearby wastewater disposal well (now decommissioned). Both Progress Energy and CNRL stations were equipped with three-component broadband sensors (nominal flat velocity response from 40 s to 50 Hz) and 24-bit digitizers (8 peak-to-peak voltage).

Figure 2 shows the cumulative number of seismic events in Figure 1 for which the magnitude was 3 and higher. The magnitude threshold of 3 was chosen because it is the magnitude of completeness for the NRCan earthquake catalog for this region for the time period of 1985–2013 (Babaie Mahani *et al.*, 2016). Since then, this value has been decreased by 1 unit of magnitude as a result of the installation of additional seismographic stations in NE BC and western Alberta (Salas *et al.*, 2013; Salas and Walker, 2014). It is clear in Figure 2 that the number of M 3+ events increased by a factor of ∼3 from 33 in 2008 to 97 in 2015. Recent studies in NE BC revealed that this increase appears to be specifically associated with the increase in the hydraulic fracturing operations in the area (Atkinson *et al.*, 2016).

Fluid Injection and Seismic Activity

In this study, we focus on a particular area in the NMP BC where the 17 August 2015 M_w 4.6 event occurred (black box in Fig. 1). Within our study area, different types of fluid injection operations have been taking place for decades. Figure 3 shows the monthly seismic activity and fluid injection in this area in 2015. The surface location of hydraulic fracturing and long-term injection wells are labeled in numbers and alphabets, respectively. There were 17 locations where multistage hydraulic fracturing took place episodically during 2015. Meanwhile, there are nine locations where wastewater disposal and gas injection have been active in the past 5 years. In Figure 3, F, H, and I are the three wastewater disposal wells that have been operating since 1999, 2013, and 2002, respectively. Disposal well F has been injecting water into the Mississippian Debolt Formation (limestone), whereas wells H and I have been injecting water into the Middle Triassic Halfway Formation (sandstone). The other closely spaced wells (A, B, C, D, and E) and well G have been injecting gas into the Cretaceous Gething and Bluesky Formations (sandstone) since 1987 and 2012, respectively. On the other hand, all of the multistage hydraulic fracturing operations took place along horizontal wells into the Lower Triassic Montney Formation (siltstone; see Data and Resources for more information on the sediment stratigraphy in NE BC). Ⓔ Tables S1 and S2, available in the electronic supplement to this article provide injection parameters for the locations shown in Figure 3.

The distribution of seismicity shown in Figure 3 is based on the local earthquake catalog determined from the Progress Energy seismograph network which includes 676 events from 3 October 2014 to 31 December 2015 with M_w as small as 1. The epicentral uncertainty of this catalog is less than 1 and 1.3 km in east–west and north–south directions,
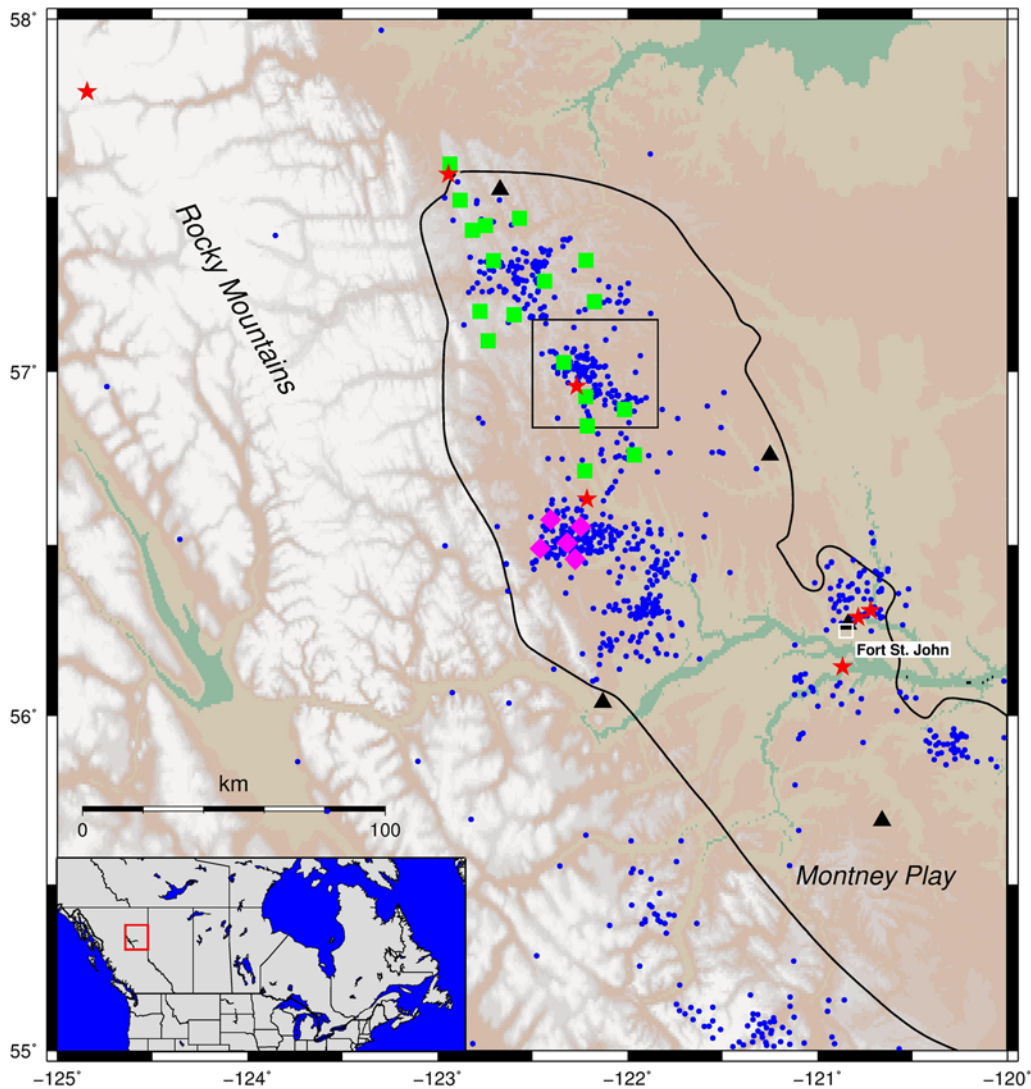
Figure 1.   Seismicity in northeast British Columbia (NE BC) from 1985 to 2016 from the Natural Resources Canada (NRCan) earthquake catalog (dots). The inset shows the region in North America. The triangles, solid squares, and diamonds show the location of the regional, Progress Energy, and Canadian Natural Resources Limited seismographic stations, respectively. Stars show events with magnitude 4 and higher. The black box shows our study area in Figure 3. The color version of this figure is available only in the electronic edition.

respectively. On the other hand, the average epicentral uncertainty in the NRCan catalog can be ~2 km (and more in the east–west direction) in this area (Babaie Mahani *et al.*, 2016). The depth uncertainty of these catalogs, however, is larger (e.g., as large as 5 km for the Progress Energy catalog) and not suitable for studying shallow induced events.

Another noticeable difference between the NRCan and Progress Energy catalogs is the magnitude scale. Although M_w is reported by Progress Energy, most events in the NRcan catalog are given the local magnitude (M_L), except for a small number of relatively large events whose regional moment tensor solutions can be inverted (Kao *et al.*, 2012). Babaie Mahani *et al.* (2016) compared the M_L values reported in the NRCan catalog to the M_w values in the Progress Energy catalog using similar datasets for NMP BC. A general trend is that the NRCan local magnitude tends to be

higher than the Progress Energy moment magnitude, which can be due to the different magnitude types and frequency band used in the magnitude calculation, sensors and instruments, site conditions, network geometry, and processing procedures of earthquake signals (Babaie Mahani *et al.*, 2016). For example, the 17 August 2015 event was given an M_w of 4.1 in the Progress Energy catalog, whereas an M_L of 4.5 was given in the NRCan catalog. Ⓔ Table S3 provides seismicity catalog used in this study.

Given the previously described concatenation between input catalogs, we investigate the spatial and temporal relationship between fluid injection and seismicity in the study area. From Figure 3, we can observe several characteristics in seismicity during 2015 in this region. First, the seismicity pattern is different before and after August. With the exception of the month of February, much of seismicity appears to
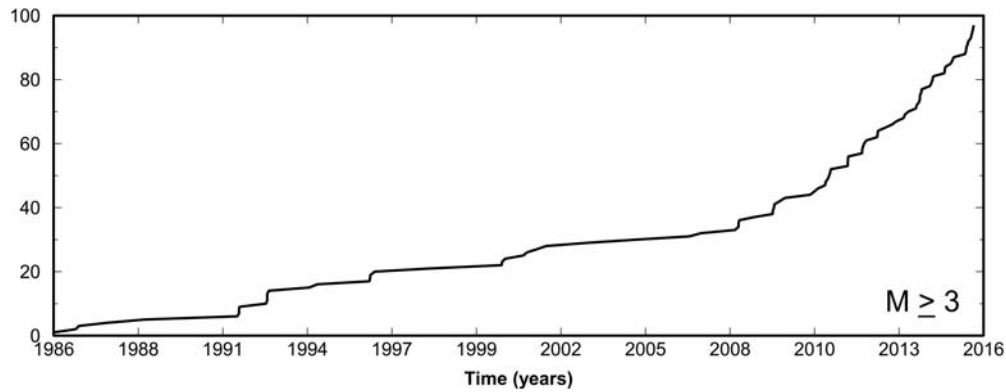
Figure 2. Cumulative number of seismic events with magnitude 3 and higher in the NE BC region (Fig. 1). A threefold increase in the number of events has been observed since 2008.

be sporadic throughout the region before August. On the other hand, after August 2015, we can see that seismicity is clustered in the northwest–southeast direction, compatible with the orientation of faults within the RMFTB (Thompson, 1989). Moreover, the number of seismic events increased significantly since August. Because the number of seismic stations in the Progress Energy network remained the same (18 stations; Fig. 1), the increase in the number of seismic events must be due to the occurrence of events rather than increase in the network capability to record more events.

Second, with the exception of the wastewater disposal well F in February, seismicity appears to be better correlated with the location of hydraulic fracturing wells than other types of fluid injection. There are almost no seismic events associated with the location of gas injection wells A–E, G, and wastewater disposal wells H and I throughout the year (Fig. 3). There are also clusters that show little spatial correlation with the sites of fluid injection (e.g., cluster to the southwest of disposal well F in March and cluster to the south of hydraulic fracturing well 8 in November).

To better understand the relationship between seismicity and fluid injection, we analyzed the volume of injected fluid from wells shown in Figure 3. Figure 4 shows injection volumes for hydraulic fracturing, wastewater disposal, and gas injection wells in 2015. Among the injection wells A–I, the higher injection volumes were from gas injection wells C and D, which had monthly injection of up to $\sim 100{,}000$ m^3 (Fig. 4a). On the other hand, monthly injection volume from disposal wells F and H reached to the maximum value of only ~ 3000 m^3. Wells A, G, and I did not inject during 2015, therefore, are not shown in Figure 4a. Although injection volumes from hydraulic fracturing wells were less than ~ 2300 m^3 per stage (Fig. 4b), hundreds of stages were performed along horizontal wells. For example, hydraulic fracturing well 10, which is associated with seismicity in August and September (Fig. 3), had 132 stages from 11 August to 8 September and injected more than $160{,}000$ m^3 during this period (Ⓔ Table S1). Before the occurrence of the M_w 4.6 event on 17 August, this well had injected more than $65{,}000$ m^3 of fluid in only 6 days.

An interesting observation from Figures 4c and 5 is the correlation of maximum magnitude and cumulative number of seismic events with hydraulic fracturing. In Figure 4c, we note a decrease in the daily maximum magnitude during time intervals with less intensive hydraulic fracturing operations. A similar trend can be observed in Figure 5, which shows the cumulative number of events and hydraulic fracturing stages. There is an apparent match between increase in the number of hydraulic fracturing stages and increase in the number of seismic events. There were two sharp increases in the number of hydraulic fracturing stages, as can be seen in Figure 5. The first increase happened on 11 November 2014 followed by the second increase on 4 July 2015. Similarly, seismicity increased steadily until 1 February 2015 when the first significant increase in the number of seismic events is observed. The second significant increase in the number of seismic events occurred on 15 August 2015, two days before the occurrence of the M_w 4.6 event.

Based on the spatial and temporal correlation of seismicity with fluid injection, along with the analysis of individual and total volumes from each injection well, it is strongly suggested that seismic activity in the NMP BC during 2015 was more related to local hydraulic fracturing than other sources of injection.

Statistical Correlation between Hydraulic Fracturing and Seismicity

In the Fluid Injection and Seismic Activity section, we showed that seismicity is preferentially located nearby hydraulic fracturing wells. To further investigate the correlation between fluid injection from hydraulic fracturing and seismicity in a more robust manner, we performed a statistical cross-correlation test between earthquakes and hydraulic fracturing operations (Telesca, 2010; Oprsal and Eisner, 2014). The results of this analysis (Fig. 6a) compare the earthquake catalog time series (daily earthquake counts) with the reported daily injection volumes for all hydraulic fracturing wells in the study region. In Figure 6a, seismic activity and injection volumes from hydraulic fracturing wells are shown since October
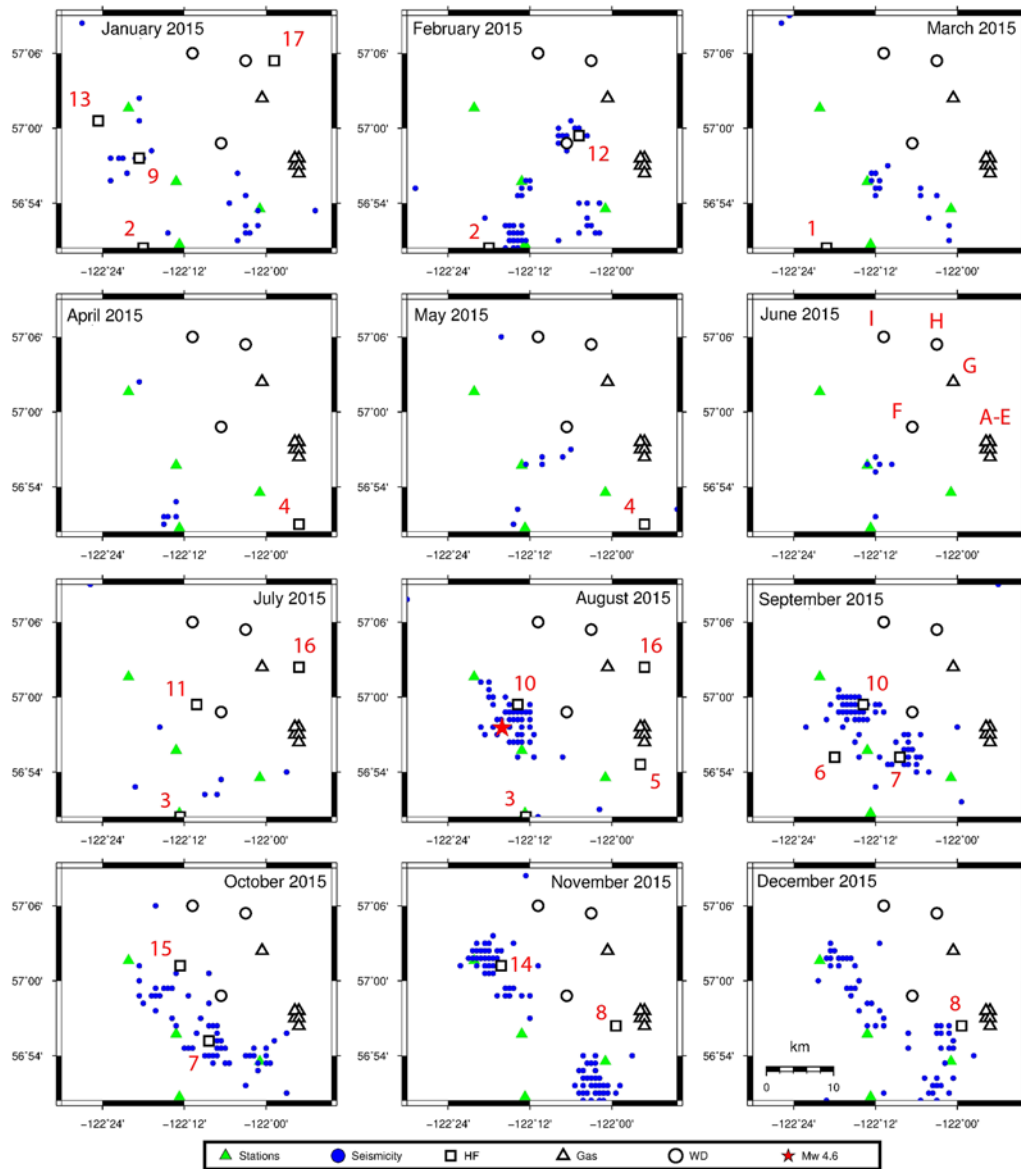
Figure 3. Monthly distribution of seismic events (dots) and location of fluid injection sites in the vicinity of the 17 August 2015 M_w 4.6 event (black box in Fig. 1) in 2015. The surface location of hydraulic fracturing and long-term injection wells are labeled by numbers (open squares) and alphabet (open triangles and open circles), respectively. HF, hydraulic fracturing; WD, wastewater disposal. The color version of this figure is available only in the electronic edition.

2014 to compare the background seismicity with the activity in 2015. Seismicity within the three-month period before 2015 was comparable to the background activity during the period in 2015 when less intensive hydraulic fracturing injection was taking place (days 50–200 in Fig. 6a). Ⓔ Figure S1 shows the location of seismicity and injection during the months of October, November, and December 2014.

To limit the impact of biases due to network detection thresholds, our seismicity catalog was truncated based on a magnitude of completeness that maximizes the likelihood objective function. In brief, we sequentially truncated the catalog using lower and lower magnitude of completeness (M_c). For each M_c, we determined the seismic b-value (Aki, 1965; Shi and Bolt, 1982; Marzocchi and Sandri, 2003),

goodness of fit (R^2), and the value of the likelihood function. M_c was chosen as the one with the best fit to the b-value. With this approach, the b-value was estimated to be 1.2 ± 0.08, with an M_c of 1.3 and R^2 of 0.889 (Fig. 6b). Our results from the statistical cross-correlation test (Fig. 6c) indicate a correlation coefficient of ∼0.17 between seismicity and hydraulic fracturing with a confidence close to 99.7% and a lag time between 0 and 2 days. This relatively low correlation coefficient is probably due to the fact that some of the seismic activity (Fig. 3 and Ⓔ Fig. S1) does not appear to be associated with any of the injection wells (hydraulic fracturing and long-term injection) in the area. In making Figure 6, we used the entire catalogs of seismicity and hydraulic fracturing injection since October 2014 to the end of
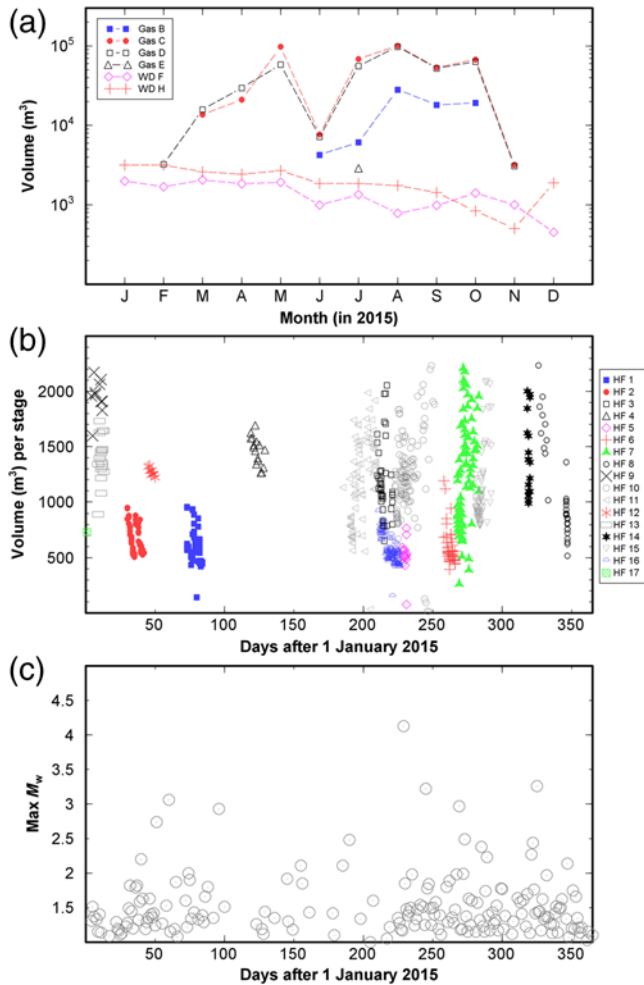
Figure 4. (a) Monthly injection volume at each wastewater disposal (WD) and gas injection well (Gas) in 2015. (b) Daily injection volume (per stage) at each hydraulic fracturing well (HF) in 2015. (c) Maximum M_w observed each day for the area shown in Figure 3. The color version of this figure is available only in the electronic edition.

2015. In other words, using seismicity associated with individual hydraulic fracturing wells would probably result in a correlation coefficient of more than ∼0.17. The lag time obtained from Figure 6c seems to be different from the longer lag times seen in Figure 5 in which the cumulative number of stages and seismicity was compared. The reason behind this discrepancy can be due to the inclusion of some of the well data in the cross-correlation test that would lead to spurious results, in the sense that hydraulic fracturing wells which are still in the bounding study box (Fig. 3) can occur 30+ km away from earthquake clusters and with large lag times of 40–50 days (e.g., wells 1, 4, 5, 11, 16, and 17 in Fig. 3). The poor temporal resolution of hydraulic fracturing parameters (daily records), however, precludes the ability to confidently determine the precise lag times between hydraulic fracturing operations and associated seismicity.

The frequency–magnitude distribution and seismic *b*-value can reveal important information regarding seismic-
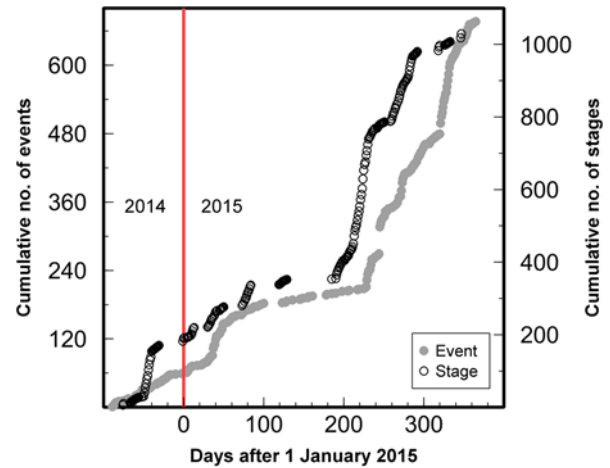

Figure 5. Cumulative numbers of seismic events and hydraulic fracturing stages. Sharp increase in seismicity correlates remarkably well with the increase in hydraulic fracturing operations. The color version of this figure is available only in the electronic edition.

ity from fluid injection. A decrease in the *b*-value with time can be indicative of the increase in likelihood of larger magnitude events. Here, we calculated the *b*-value from October 2014 to the end of 2015 for seismicity shown in Figure 3 and Ⓔ Figure S1 (Fig. 7). To ensure the validity of our *b*-value calculation, we used varying time windows with a constant M_c of 1.3 in each bin (Fig. 6b). This resulted in 13 periods with calculated *b*-values, and the results are shown in Figure 7. The errors in Figure 7 were obtained using the same methodology as in Figure 6b. There seems to be a correlation between *b*-values and injected fluid in each bin during 2015 because the lowest *b*-value was obtained during the periods 4, 5, and 6 (27 February 2015 to 22 August 2015), with the peak of injection and the occurrence of M_w 4.6 event during period 5 (∼320,000 m³ during 17 July 2015 to 22 August 2015). After these periods, we can see that the *b*-values correlated very well with the amount of injection, with the increase in *b*-values during periods with low injection volumes. Although Figure 7 can give insights into understanding the relation between fluid injection and seismic events, higher temporal resolution (e.g., hourly) for injection parameters and denser seismicity catalogs (microseismicity) are needed for more robust analysis of this kind.

Double-Difference Relocation of Earthquakes in August and September

To ascertain the relative geometry of the event hypocenters, we employed the double-difference relocation technique (Waldhauser and Ellsworth, 2000; Waldhauser, 2001) for some events for which both the regional and local industry-provided waveforms in August and September of 2015 were available. First, events were relocated using conventional methods (Pavlis *et al.*, 2004) and a local velocity model (Laske *et al.*, 2013; Table 1). The addition of industry-
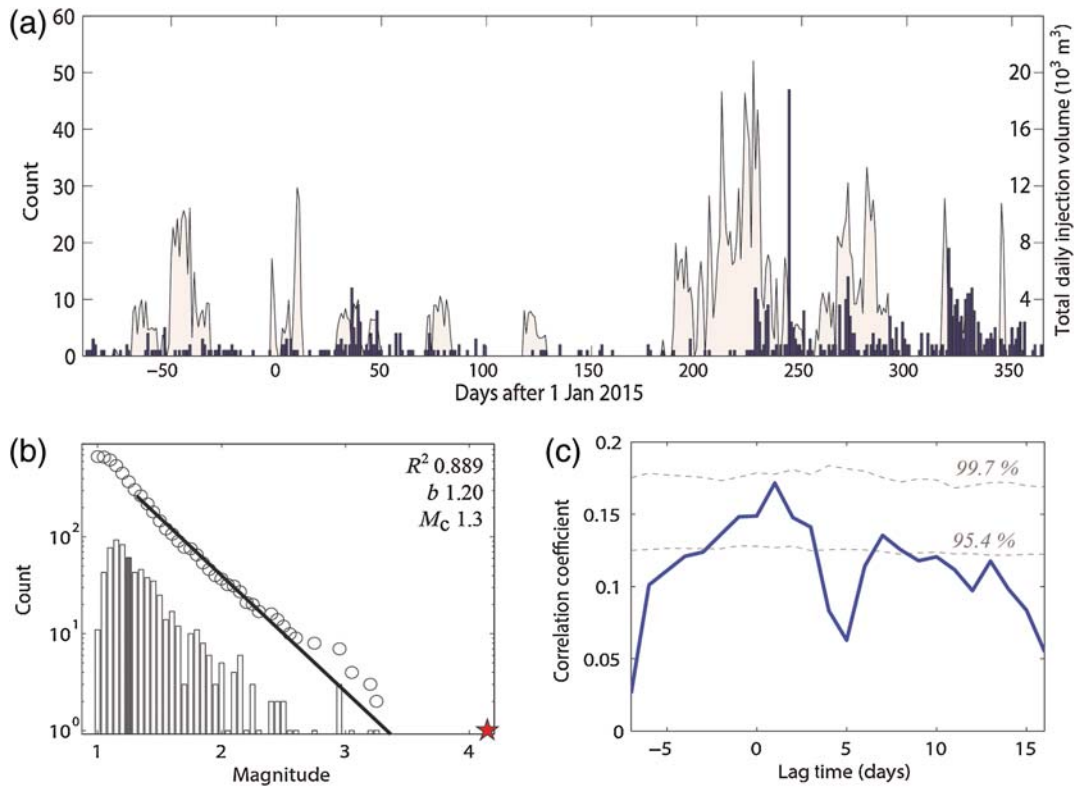
Figure 6. Hydraulic fracturing operations and local seismicity in the study area for the period October 2014 to the end of 2015. (a) Daily counts of earthquakes and injection volume for all hydraulic fracturing wells (Fig. 3 and Ⓔ Fig. S1, available in the electronic supplement to this article) are shown as solid bars and gray areas, respectively. (b) Maximum-likelihood fit (solid line) to the Gutenberg–Richter relationship of local seismicity. Histogram and circles show the probability density function and cumulative density function of the Gutenberg–Richter plot, respectively. Star shows M_w 4.6 (M_w 4.1 in the Progress Energy catalog used in making this figure) which was not considered in the calculation of the b-value. M_c, magnitude of completeness; R^2, goodness of fit. (c) Statistical cross-correlation test between the time series of earthquakes and hydraulic fracturing operations in (a). Dashed lines mark the computed confidence intervals. The color version of this figure is available only in the electronic edition.

provided, broadband data is crucial to improve station coverage at local distance (∼5–50 km), which constrain events within 0–5 km focal depth. Despite the inclusion of this local data, focal depths remained fixed at 2 km during our conventional relocations; a reasonable starting guess in light of the stimulation depth from nearby hydraulic fracturing opera-
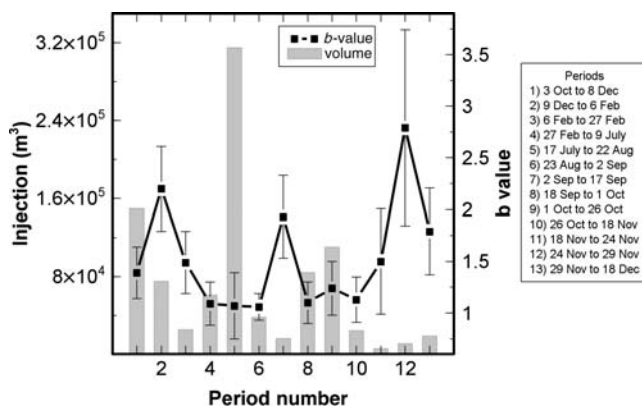

Figure 7. Injection volume from hydraulic fracturing operations and seismic b-value from October 2014 to the end of 2015.

tions. This relocation provided an input catalog of 29 events with up to 22 phase picks each for double-difference inversion. In total, the phase arrival pairings of these events produced more than 2400 catalog and 500 waveform differential lag times. To ensure the validity of our relocation results, we performed 1000 bootstrap tests (Efron and Tibshirani, 1986), in which 10% of the catalog is randomly removed before double-difference inversion was repeated. These tests allowed us to more accurately determine hypocentral parameters and their uncertainties through the statistical distribution of test locations. After this procedure, 22 determined hypocenters were obtained (Fig. 8). Figure 8 shows that these events are predominantly centered around the M_w 4.6 earthquake which occurred at a distance of ∼1.5 km to the southwest of the Progress Energy hydraulic fracturing injection pad (well 10 in Fig. 3). Laterally, our relocations constrain events to a subhorizontal planar geometry with an apparent area of ∼21 km².

Furthermore, to test the validity of our initial choice for focal depth, we performed additional double-difference inversions with perturbed initial depth guesses. Initial guesses of focal depth were chosen between 1 and 6 km. Overall, we
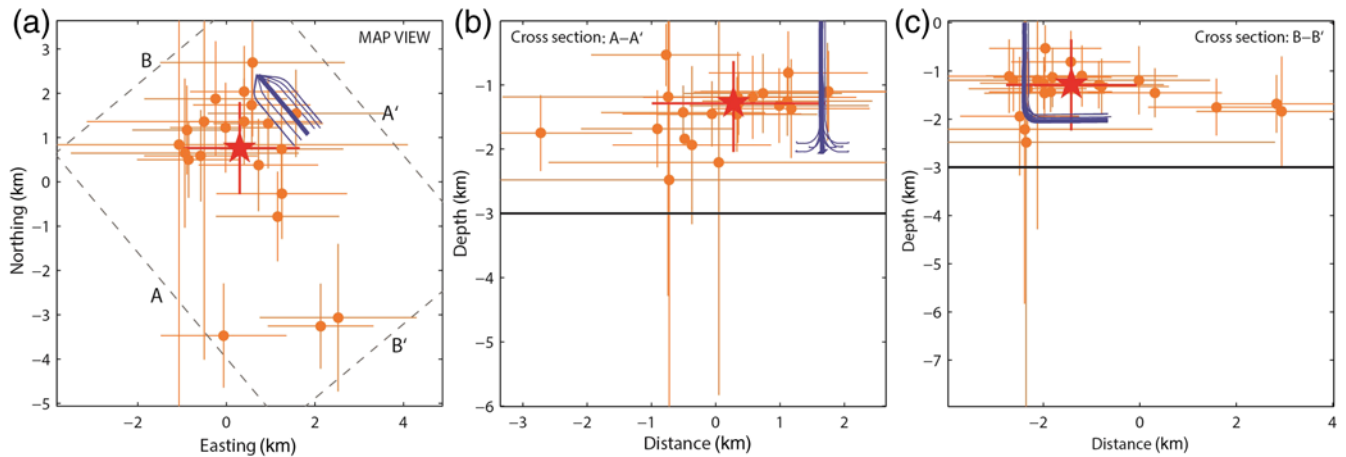
Figure 8. Results of the double-difference inversion. Solid circles are the double-difference earthquake relocations. Hypocentral location of the 17 August 2015 M_w 4.6 event is denoted by a star. Error bars at each earthquake location mark the 95% confidence interval. Lines show the location and geometry of hydraulic fracturing wells at one of the Progress Energy pads (well 10 in Fig. 3), with the bold line being the well, which had perforation dates contemporaneous with the M_w 4.6 event. (a) Top-down map view; (b) southwest–northeast cross section; and (c) northwest–southeast cross section. The bold horizontal line marks the depth to basement. The color version of this figure is available only in the electronic edition.

found that the constraints on the centroid focal depth largely mirror the input guess values as double-difference methods often have problems determining absolute locations (Waldhauser and Ellsworth, 2000), which reduces our ability to constrain depth with fidelity. However, we do note that inversions become increasingly unstable with initial guesses below a focal depth of 2 km. Likely, this instability is a result of poorer initial guesses. Assuming an initial focal depth of 2 km, focal depth inversions were found to be mainly above the injection target depth, with the deepest events reaching a depth of 2.5 km (Fig. 8b,c). However, given these hypocentral uncertainties, we hesitate to further interpret the focal depth determinations of these events. We note that high resolution datasets such as downhole microseismic ones would be required to place better constraints on the true focal depth of these events.

Moment Tensor Inversion of the M_w 4.6 Event

The 17 August 2015 M_w 4.6 earthquake is the largest event that occurred in the NMP BC because the local shale gas development began approximately a decade ago. The NRCan first determined its M_L as 4.5, based on amplitude measurements at 15 Canadian National Seismograph Network (CNSN) stations. A preliminary moment tensor solution with an M_w of 4.6 was later obtained by inverting CNSN waveforms recorded at regional distances. In this study, we incorporated broadband waveform data from the local seismographic stations into the moment tensor inversion for the M_w 4.6 earthquake. The same velocity model used in previous moment tensor inversion for regional earthquakes in western Canada as specified in Kao *et al.* (2012; Table 2) was adopted. Both the observed and synthetic waveforms were filtered at the 0.02–0.1 Hz frequency range using a

second-order Butterworth band-pass filter. Moment tensor inversions usually involve deconvolution of the observed data from the instrument response (Jost and Herrmann, 1989; Ekstrom *et al.*, 2012). This process would often introduce very large long-period noise when the size of the earthquake is smaller than M 6. This is particularly worse for the horizontal components (radial and transverse). To effectively eliminate this drawback, we decided to convolve the synthetic waveforms (in ground displacement) for each station with the corresponding instrument response first before they are used to construct the inversion kernel. Using this approach, we managed to use horizontal components from many stations for the 17 August 2015 M_w 4.6 event, thus imposing more constraint to the inversion results. In some cases, the extra constraint from these additional waveforms makes it impossible to find an acceptable solution at some depths. This is in sharp contrast to a broad misfit curve without good depth resolution. In other words, the added capacity in our inversion to use more waveform data has significantly improved the resolution of the inversion results.

The inversion was repeated for a ±12-km range around the initially reported focal depth, and the best solution was determined by choosing the one with the lowest overall misfit. The results of the moment tensor inversion are shown in Figure 9. The best solution corresponds to a thrust mechanism with northwest–southeast nodal planes. The focal depth for this solution is 4 km, which is deeper than the value obtained through double-difference relocation (1.3 km). The 2.7 km difference between depth estimations for the M_w 4.6 event shows that determining the absolute depth can be highly dependent on the assumptions made during the calculation of depth, including velocity models, initial guess of depth, etc. Our M_w value (4.55) is slightly smaller than that of the preliminary NRCan moment tensor solution. Given the
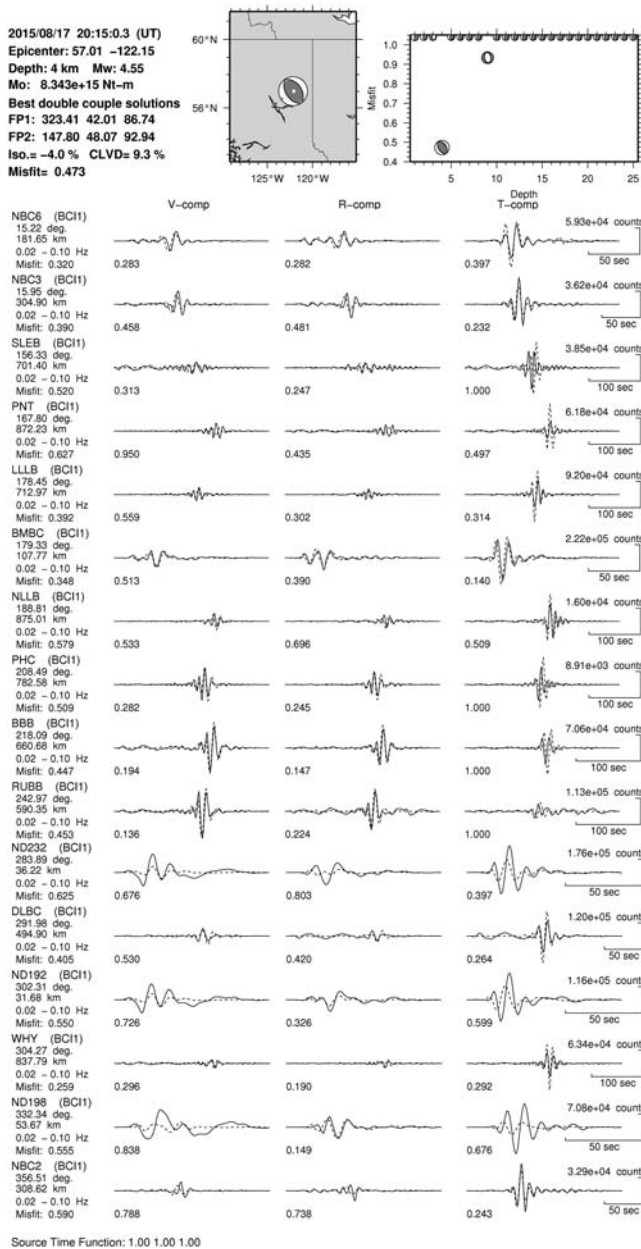
Figure 9. Moment tensor inversion for the M_w 4.6 event on 17 August 2015. A summary of source parameters, map of the epicenter, and the misfit versus depth plot are shown at the top. Epicenter location is from the NRCan catalog. Focal mechanism is plotted in lower-hemisphere projection with darkened quadrants showing compressional (up) first motions. In the lower panel, synthetic and observed seismograms at each station component used in this inversion are plotted as dashed and solid lines, respectively. V, R, and T, correspond to the vertical, radial, and transverse components, respectively.

possible uncertainty due to different datasets used in the two solutions, however, such a small difference is negligible.

The focal mechanism of the M_w 4.6 event shows little non-double-couple components (isotropic and compensated linear vector dipole). The orientation of P and T axes is consistent with the orientation of the maximum horizontal stress in this area, indicative of a compressional regime (Heidbach

Table 1
Velocity Model Used in Double-Difference Relocations
(Laske *et al.*, 2013)

Depth (km)	V_P (km/s)
0.0	4.6
3.0	6.3
19.4	6.6
33.8	7.0
42.0	8.1

Table 2
Velocity Model Used in Moment Tensor Inversion

Thickness (km)	V_P (km/s)	V_S (km/s)	ρ (g/cm^3)	Q_P	Q_S
1	4.8	2.8	1.8	500	250
2	5.5	3.2	2.2	500	250
5	6.1	3.5	2.3	500	250
17	6.2	3.6	2.7	500	250
8	6.5	3.7	2.9	500	250
120	8.1	4.7	3.0	500	250

et al., 2010). Similar thrust mechanisms were obtained for events in Alberta close to the RMFTB (Wetmiller, 1986; Baranova *et al.*, 1999), but events further from the deformation front show different mechanisms with more strike-slip and normal-faulting components (Eaton and Babaie Mahani, 2015; Wang *et al.*, 2015; Zhang *et al.*, 2016).

Discussion

In this study, we investigated the relationship between seismicity and several types of fluid injection operations: short-term, high-volume hydraulic fracturing, long-term, low-volume wastewater disposal, and long-term high-volume gas injection. Our purpose was to understand the occurrence of seismicity with regard to each of these injection sources, specifically their relationship to the occurrence of larger magnitude events such as the M_w 4.6 on 17 August 2015, which was found to be strongly correlated in space and time with the hydraulic fracturing operations than other types of injection.

Although our investigation of the spatiotemporal correlation between injection and seismicity was focused only for 2015, we note that disposal wells in the area have been operating for decades. The geographically widespread effect of long-term wastewater disposal has been the main conclusion of the observed induced seismicity for events as large as M_w 5.6 in the United States (Keranen *et al.*, 2013; Rubinstein and Babaie Mahani, 2015). In contrast to the short-term injection from hydraulic fracturing operations, decades of injection for wastewater disposal expand the affected overpressured area, making it more likely to intercept faults at larger distances from the injection point (Keranen *et al.*, 2014). However, the injected volume from disposal wells in our study area is very low compared to those in the United States,

which have been associated with the increase in the occurrence of seismic activity. The highest-volume wastewater disposal well in our study area is well F, ∼10 km in the northeast of the M_w 4.6 event, which has been injecting since 1999 with maximum monthly volume of ∼2200 m³, reaching a total volume of only more than 200,000 m³ in 16 years (Ⓔ Table S2). In contrast, the largest disposal well in southeast Oklahoma City, associated with the increase in the rate of seismicity in the region, injected up to 1.6 million barrels of fluid (∼250,000 m³) per month during 2004–2012 (Keranen *et al.*, 2014), which is ∼114 times higher than the monthly injection volume from disposal well F in Figure 3. This difference in the injection volumes is also observed at other disposal wells in western Canada (Schultz *et al.*, 2014) and should be taken into account when addressing induced seismicity in the United States and Canada, especially with regard to larger magnitude events. Unfortunately, the sparsely covered regional seismograph network in NMP BC prevents a long-term correlation of seismicity with injection in this area, especially before 2013 when there were only two broadband stations in the entire NE BC region.

Conclusion

In this study, we analyzed the relation between fluid injection and seismic activity in the northern Montney Play of British Columbia in 2015. We used an industry-provided seismicity catalog including 676 events from 3 October 2014 to 31 December 2015, with moment magnitudes as small as 1. Based on the spatial and temporal correlation of seismic activity with fluid injection in the region and higher injection volumes from hydraulic fracturing operations than disposal wells, we found that the occurrence of local events is better correlated with hydraulic fracturing operations. Using the double-difference relocation technique, we obtained hypocentral constraints for events in August and September. Focal depths of the studied events are located mainly above the injection target zone, ranging from 0.5 to 2.5 km. The 17 August 2015 earthquake had a moment magnitude of 4.6, with its epicenter located at a distance of ∼1.5 km to the southwest of a hydraulic fracturing pad operated by Progress Energy. Results of the moment tensor inversion of this event revealed a thrust focal mechanism on nodal planes striking northwest–southeast. This solution is compatible with the orientation and mechanism of pre-existing faults in the Rocky Mountain fold-and-thrust belt.

Data and Resources

Information on the 17 August 2015 earthquake was obtained from the Natural Resources Canada (NRCan) earthquake catalog and can be seen at http://earthquakescanada.nrcan.gc.ca/ (last accessed December 2016). Information on the sediment stratigraphy in northeast British Columbia can be obtained from http://www2.gov.bc.ca/gov/content/industry/natural-gas-oil/petroleum-geoscience/sedimentary-basins-of-bc/northeastern-bc-basin (last accessed December 2016). The Alberta Energy Regulator subsurface order number 2 can be obtained from https://aer.ca/documents/orders/subsurface-orders/SO2.pdf (last accessed December 2016). Analysis of seismicity in the Montney Trend can be seen at https://www.bcogc.ca/node/12291/download (last accessed December 2016). The Montney Formation Play Atlas northeast British Columbia (NE BC) can be obtained from http://www.bcogc.ca/node/8131/download (last accessed December 2016). Report on the Ultimate Potential for Unconventional Petroleum from the Montney Formation of British Columbia and Alberta is available at https://www.neb-one.gc.ca/nrg/sttstc/ntrlgs/rprt/ltmtptntlmntnyfrmtn2013/ltmtptntlmntnyfrmtn2013-eng.pdf (last accessed December 2016).

References

Aki, K. (1965). Maximum likelihood estimate of b in the formula $\log(N) = a - bM$ and its confidence limits, *Bull. Earthq. Res. Inst.* **43,** 237–239.

Atkinson, G. M., D. Eaton, H. Ghofrani, D. Walker, B. Cheadle, R. Schultz, R. Scherbakov, K. Tiampo, Y. J. Gu., R. Harrington, *et al.* (2016). Hydraulic fracturing and seismicity in the western Canada sedimentary basin, *Seismol. Res. Lett.* **87,** 631–647.

Atkinson, G. M., H. Ghofrani, and K. Assatourians (2015). Impact of induced seismicity on the evaluation of seismic hazard: Some preliminary considerations, *Seismol. Res. Lett.* **86,** 1009–1021.

Babaie Mahani, A., H. Kao, D. Walker, J. Johnson, and C. Salas (2016). Performance evaluation of the regional seismograph network in northeast British Columbia, Canada, for monitoring of induced seismicity, *Seismol. Res. Lett.* **87,** 648–660.

Baranova, V., A. Mustaqeem, and S. Bell (1999). A model for induced seismicity caused by hydrocarbon production in the western Canada sedimentary basin, *Can. J. Earth Sci.* **36,** 47–64.

Eaton, D. W., and A. Babaie Mahani (2015). Focal mechanisms of some inferred induced earthquakes in Alberta, Canada, *Seismol. Res. Lett.* **86,** 1078–1085.

Efron, B., and R. Tibshirani (1986). Bootstrap methods for standard errors, confidence intervals, and other measures of statistical accuracy, *Stat. Sci.* **1,** 54–75.

Ekstrom, G., M. Nettles, and A. M. Dziewonski (2012). The Global CMT project 2004–2010: Centroid-moment tensors for 13017 earthquakes, *Phys. Earth Planet. In.* **200/201,** 1–9.

Farahbod, A. M., H. Kao, D. M. Walker, and J. F. Cassidy (2015). Investigation of regional seismicity before and after hydraulic fracturing in the Horn River basin, northeast British Columbia, *Can. J. Earth Sci.* **52,** 112–122.

Heidbach, O., M. Tingay, A. Barth, J. Reinecker, D. Kurfeß, and B. Müller (2010). Global crustal stress pattern based on the World Stress Map database release 2008, *Tectonophysics* **482,** 3–15.

Horner, R. B., J. E. Barclay, and J. M. Macrae (1994). Earthquakes and hydrocarbon production in the Fort St. John Area of northeastern British Columbia, *Can. J. Explor. Geophys.* **30,** 38–50.

Jost, M. L., and R. B. Herrmann (1989). A student's guide to and review of moment tensors, *Seismol. Res. Lett.* **60,** 37–57.

Kao, H., S.-J. Shan, A. Bent, C. Woodgold, G. Rogers, J. F. Cassidy, and J. Ristau (2012). Regional centroid-moment-tensor analysis for earthquakes in Canada and adjacent regions: An update, *Seismol. Res. Lett.* **83,** 505–515.

Keranen, K. M., H. M. Savage, G. A. Abers, and E. S. Cochran (2013). Potentially induced earthquakes in Oklahoma, USA: Links between wastewater injection and the 2011 M_w 5.7 earthquake sequence, *Geology* **41,** 699–702.

Keranen, K. M., M. Weingarten, G. A. Abers, B. A. Bekins, and S. Ge (2014). Sharp increase in central Oklahoma seismicity since 2008 induced by massive wastewater injection, *Science* **345,** 448–451.

Laske, G., G. Masters, Z. Ma, and M. E. Pasyanos (2013). Update on CRUST1.0—A 1-degree global model of Earth's crust, *Geophys. Res. Abstr.* **15,** EGU2013–2658.

Marzocchi, W., and L. Sandri (2003). A review and new insights on the estimation of the b-value and its uncertainty, *Ann. Geophys.* **46,** 1271–1282.

Oprsal, I., and L. Eisner (2014). Cross-correlation—An objective tool to indicate induced seismicity, *Geophys. J. Int.* **196,** 1536–1543.

Pavlis, G. L., F. Vernon, D. Harvey, and D. Quinlan (2004). The Generalized Earthquake-Location (GENLOC) package: An earthquake-location library, *Comput. Geosci.* **30,** 1079–1091.

Rubinstein, J. L., and A. Babaie Mahani (2015). Myths and facts on wastewater injection, hydraulic fracturing, enhanced oil recovery, and induced seismicity, *Seismol. Res. Lett.* **86,** 1060–1067.

Salas, C. J., and D. Walker (2014). Update on regional seismograph network in northeastern British Columbia (NTS 094C, G, I, O, P), *Geoscience BC Summary of Activities 2013, Geoscience BC, Report 2014-1,* 123–126.

Salas, C. J., D. Walker, and H. Kao (2013). Creating a regional seismograph network in northeast British Columbia to study the effect of induced seismicity from unconventional gas completions (NTS 094C, G, I, O, P), *Geoscience BC Summary of Activities 2012, Geoscience BC, Report 2013-1,* 131–134.

Schultz, R., S. Mei, D. Pană, V. Stern, Y. J. Gu, A. Kim, and D. Eaton (2015). The Cardston earthquake swarm and hydraulic fracturing of the Exshaw formation (Alberta Bakken play), *Bull. Seismol. Soc. Am.* **105,** 2871–2884.

Schultz, R., V. Stern, and Y. J. Gu (2014). An investigation of seismicity clustered near the Cordel Field, west central Alberta, and its relation to a nearby disposal well, *J. Geophys. Res.* **119,** 3410–3423.

Schultz, R., V. Stern, M. Novakovic, G. Atkinson, and Y. J. Gu (2015). Hydraulic fracturing and the Crooked Lake sequences: Insights gleaned from regional seismic networks, *Geophys. Res. Lett.* **42,** 2750–2758.

Shi, Y., and B. A. Bolt (1982). The standard error of the magnitude–frequency b value, *Bull. Seismol. Soc. Am.* **72,** 1677–1687.

Telesca, L. (2010). Analysis of the cross-correlation between seismicity and water level in the Koyna Area of India, *Bull. Seismol. Soc. Am.* **100,** 2317–2321.

Thompson, R. I. (1989). Stratigraphy, tectonic evolution and structural analysis of the Halfway River map area (94B), northern Rocky Mountains, British Columbia, *Geological Survey of Canada, Memoir,* Vol. 425, 119 pp.

Waldhauser, F. (2001). HypoDD: A computer program to compute double-difference earthquake locations, *U.S. Geol. Surv. Open-File Rept. 01-113,* 25 pp.

Waldhauser, F., and W. L. Ellsworth (2000). A double difference earthquakes location algorithm: Method and application to the northern Hayward fault, California, *Bull. Seismol. Soc. Am.* **90,** 1353–1368.

Wang, R., Y. J. Gu, R. Schultz, A. Kim, and G. Atkinson (2015). Source analysis of a potential hydraulic fracturing induced earthquake near Fox creek, Alberta, *Geophys. Res. Lett.* **43,** 564–573.

Wetmiller, R. J. (1986). Earthquakes near Rocky Mountain House, Alberta, and their relationship to gas production facilities, *Can. J. Earth Sci.* **23,** 172–181.

Zhang, H., D. W. Eaton, G. Li, Y. Liu, and R. M. Harrington (2016). Discriminating induced seismicity from natural earthquakes using moment tensors and source spectra, *J. Geophys. Res.* **121,** 972–993.

Geoscience BC
1101-750 West Pender Street
Vancouver, British Columbia
Canada V6C 2T7
ali.mahani@mahangeo.com
        (A.B.M., C.S.)

Alberta Geological Survey
Alberta Energy Regulator
Suite, 205, 4999-98 Avenue
Edmonton, Alberta
Canada T6B 2X3
        (R.S.)

Pacific Geoscience Center
Geological Survey of Canada
9860 West Saanich Road
Sidney, British Columbia
Canada V8L 4B2
        (H.K.)

British Columbia Oil & Gas Commission
No. 300, 398 Harbour Road
Victoria, British Columbia
Canada V9A 3S1
        (D.W., J.J.)